

Supplementary Information for Aiken et al.Table S-1. Linear correlation, R^2 , from different $\sim PM_1$ measurements. AMS+R represents AMS plus refractory mass (BC, metals, soil).

	AMS+R	AMS	Neph	OPC	PAS
AMS	0.96				
Neph	0.70	0.71			
OPC	0.55	0.61	0.71		
PAS	0.74	0.70	0.86	0.84	
SMPS	0.68	0.57	0.61	0.24	0.48

Figure S-1. Map of the Mexico City Metropolitan Area and greater surroundings with all major sampling sites during MILAGRO labeled and altitude included by color. Mobile sites are mobile laboratories used as stationary monitoring sites during MILAGRO.

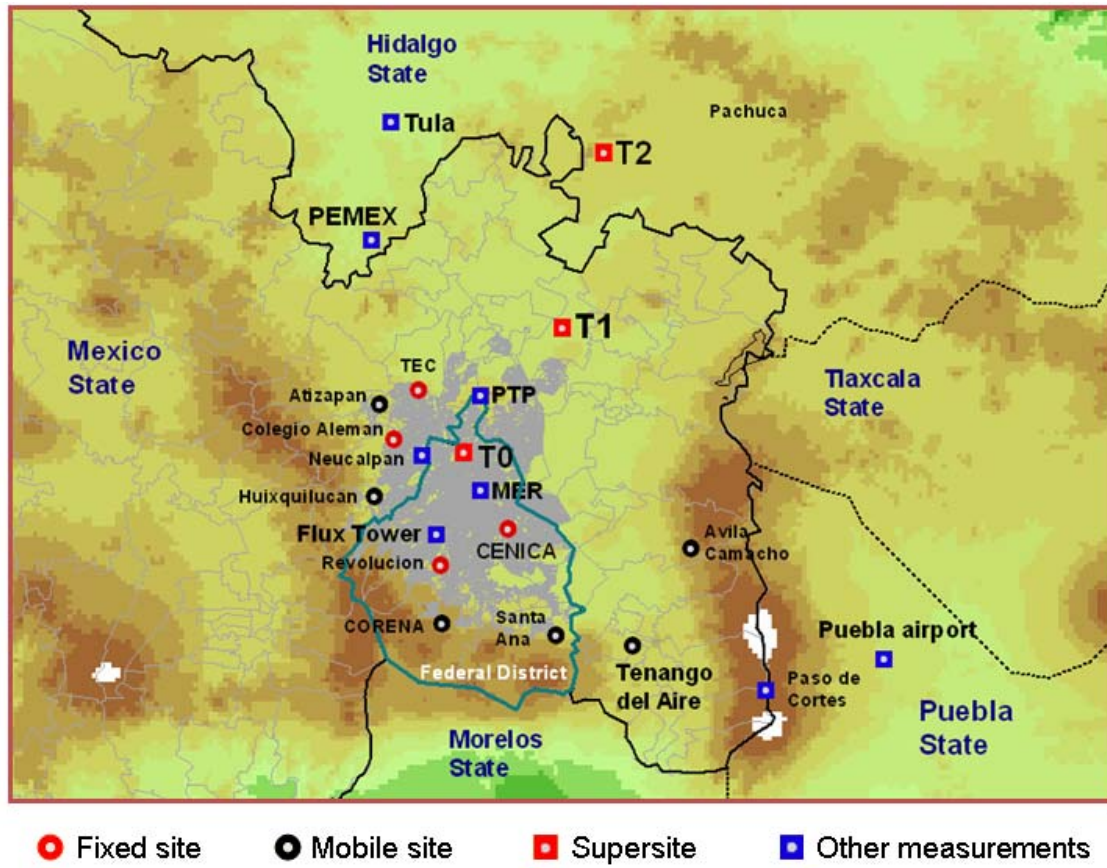


Figure S-2. SMPS volume is converted to mass using (a) a composition-dependent density to (b) compare with the mass measurements such as the AMS and others shown in Fig. S-3.

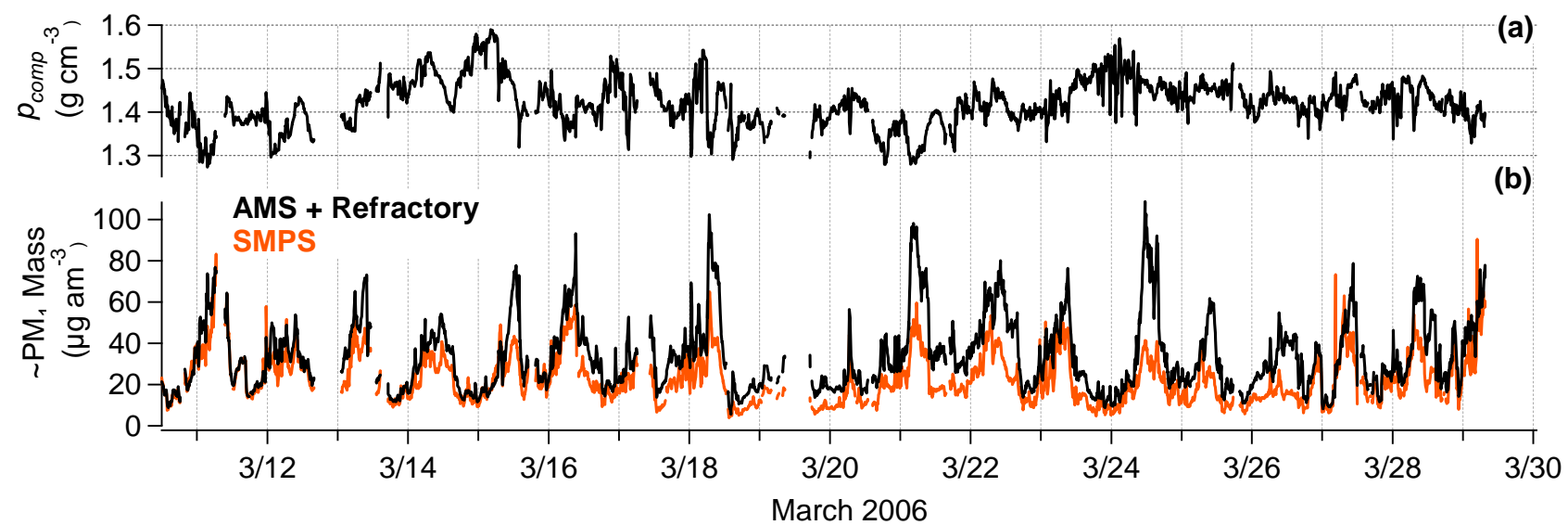


Figure S-3. $\sim\text{PM}_1$ total mass from co-located measurements. (a) Time series, and scatter plots fit by orthogonal distance regression of AMS plus refractory mass concentrations with (b) SMPS, (c) OPC, (d) nephelometer, (e) PAS reciprocal nephelometer scattering measurements at 532 nm, (f) diurnal cycles from each, (g) diurnal cycles from the OPC measurements of $\text{PM}_{2.5}$ and PM_{10} , and (h) R² values from all intercomparisons. AMS + refractory components includes BC, metals, and soil. SMPS was converted to volume using the composition-dependent density shown in Fig. S-2.

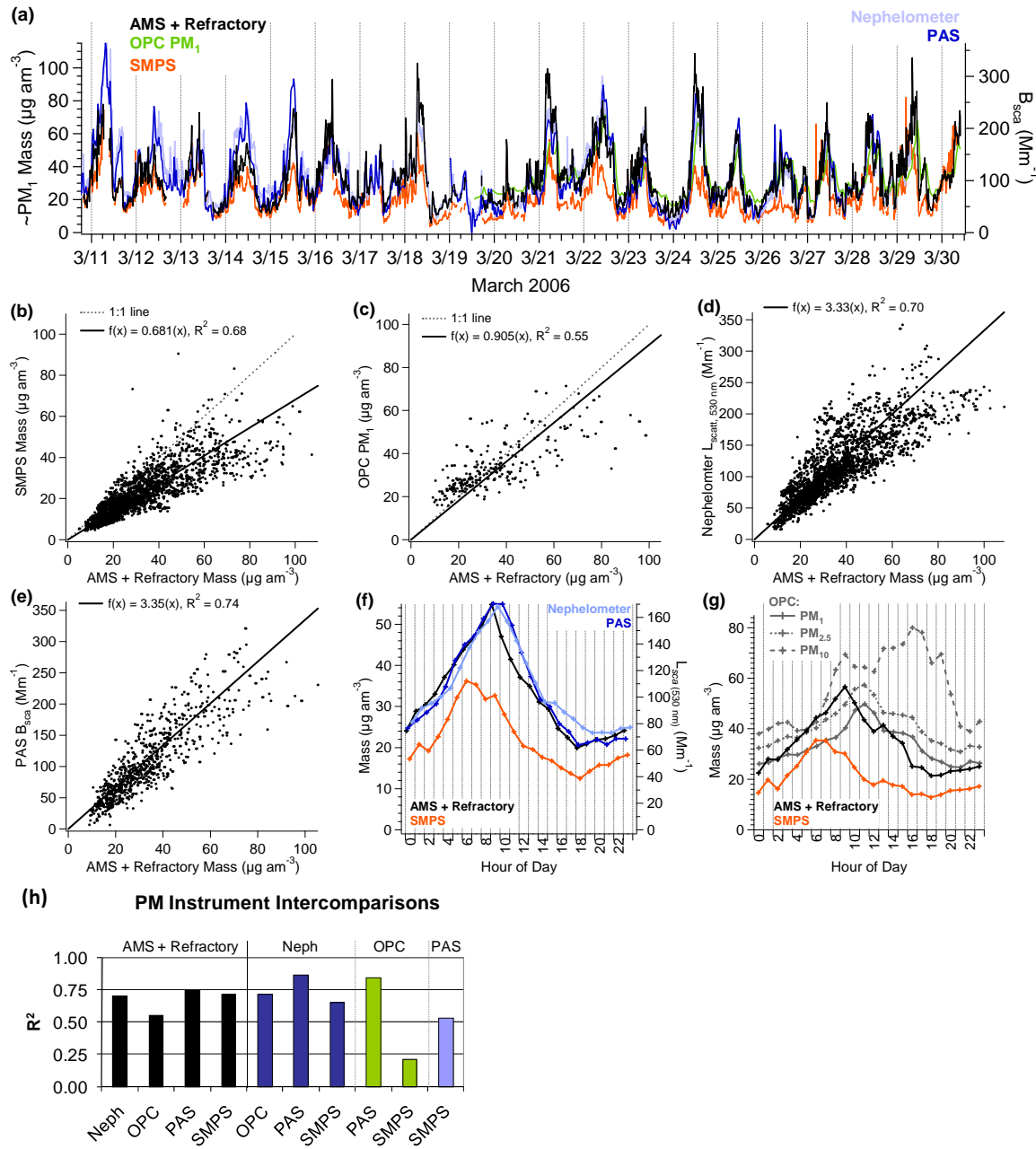


Figure S-4. Average size distributions at T0 from the AMS and AMS plus refractory species (BC, metals, soil), compared with the SMPS distribution at T0 and also with the AMS size distributions from CENICA during MCMA-2003 (Salcedo et al. 2006).

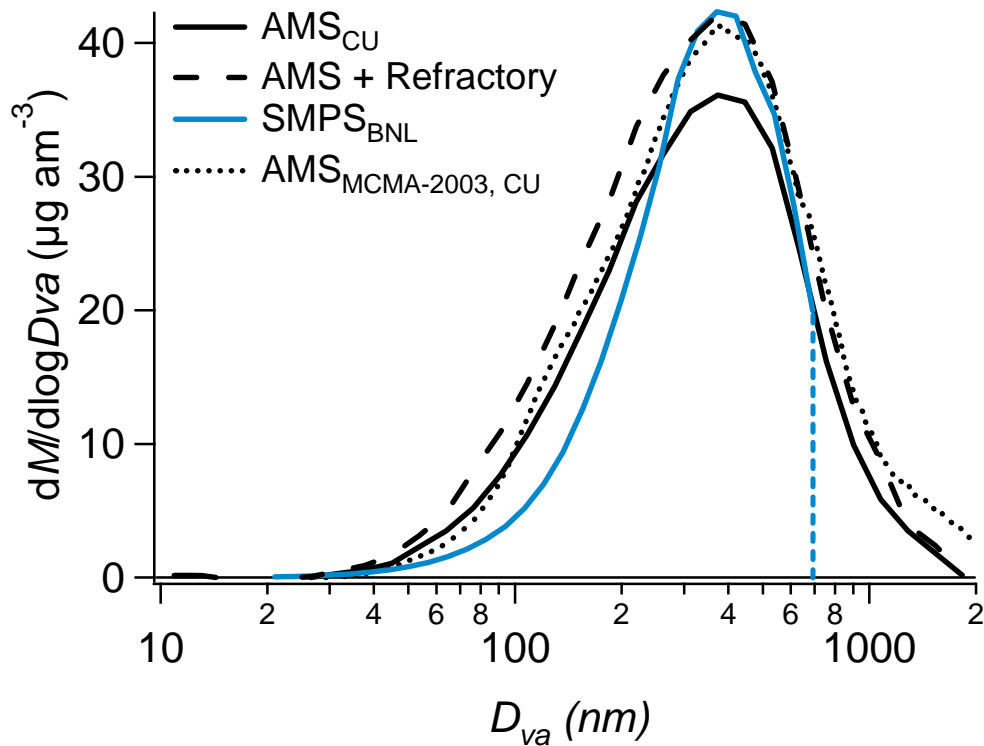


Figure S-5. Time series of (a) temperature and relative humidity, (b) precipitation, (c) particulate nitrate, and (d) mass concentrations from AMS plus refractory (BC, metals, soil) and PM₁, PM_{2.5}, PM₁₀ OPC measurements.

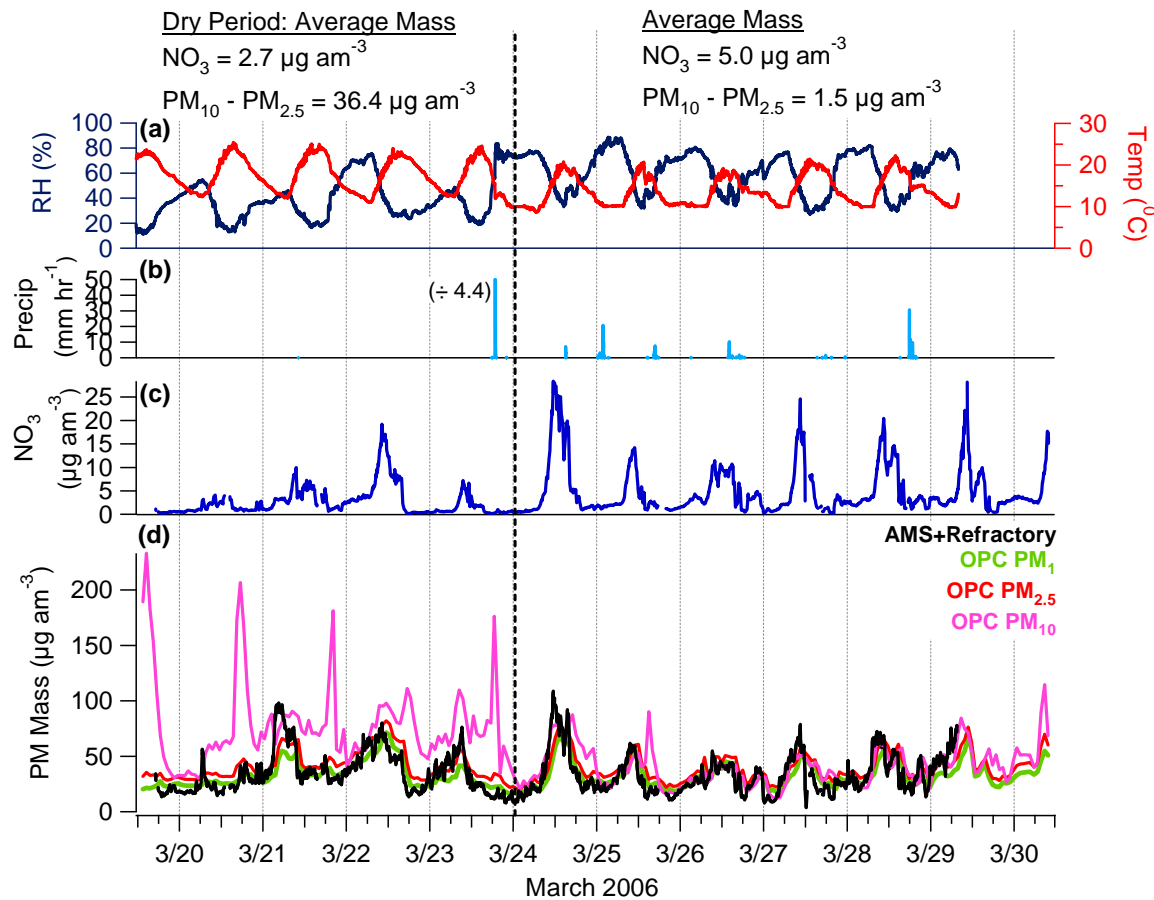


Figure S-6. Ammonium Balance (a) HR and (b) UMR with data from ammonium nitrate calibrations in black.

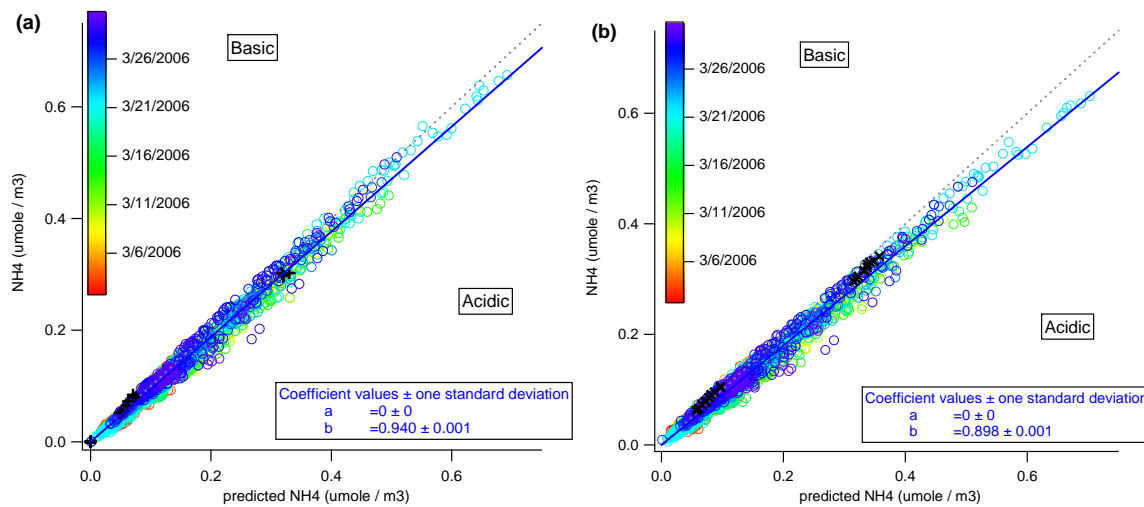


Figure S-7. Fine PM composition shown by (a) mass concentration and (b) percent for each chemical species (both refractory and non-refractory measurements).

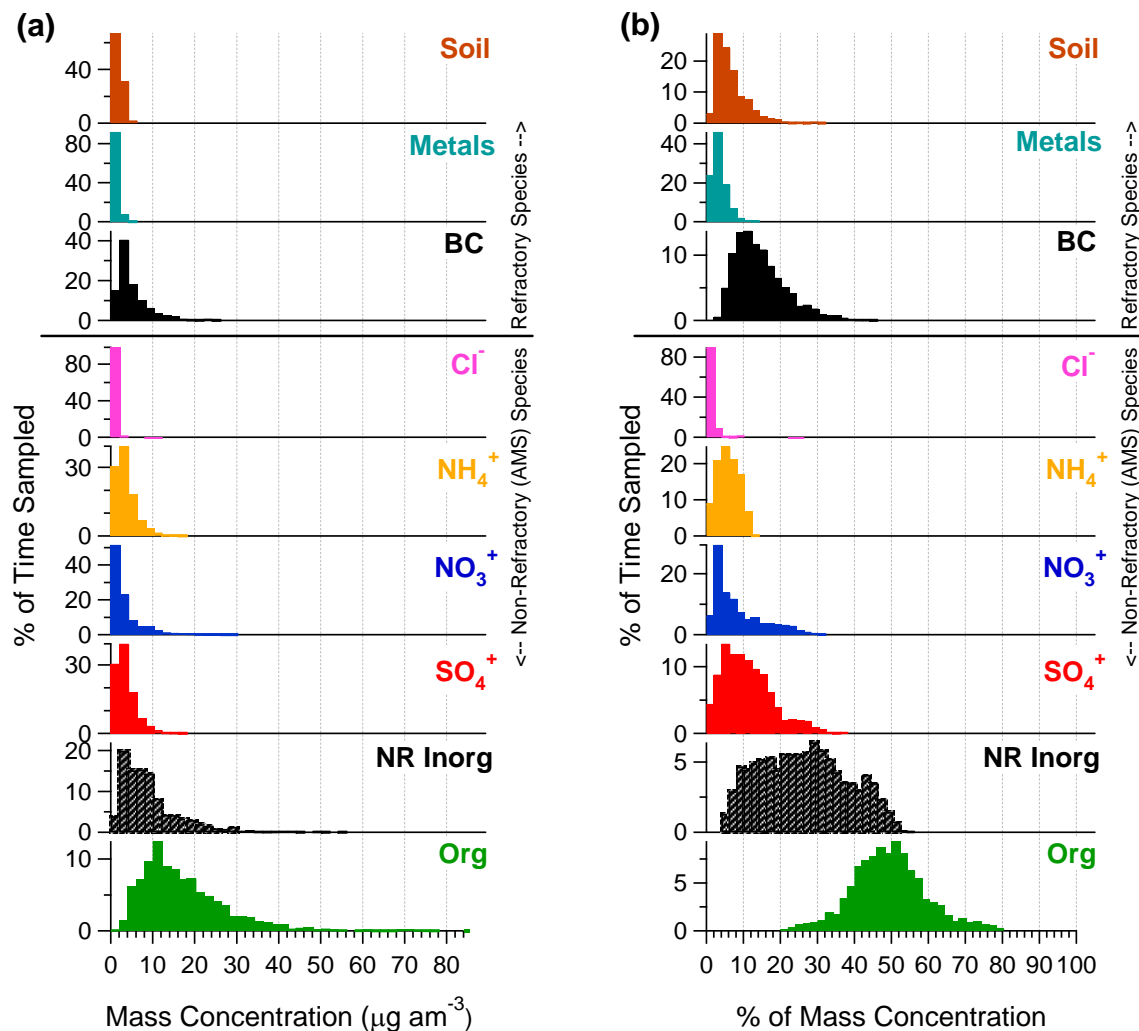


Figure S-8. Average submicron PM composition by mass ($\mu\text{g am}^{-3}$) and percent mass within the MCMA basin during different campaigns: (a) T0/IMP, NNE of downtown Mexico City (MILAGRO/MCMA-2006), (b) CENICA, E of downtown (MCMA-2003, Salcedo et al., 2006), (c) La Merced in downtown Mexico City (1997 campaign, Chow et al., 2002), (d) above the city during several afternoons in MILAGRO - C-130 aircraft, AMS only (MILAGRO/MIRAGE, DeCarlo et al. 2008). Metals are not included for the CENICA data but were lower than those at T0 due to the larger distance to the industrial sources in the N of the city (Chow et al. 2002; Salcedo et al. 2006; Moffet et al. 2008), and no refractory mass was available for the C-130 measurements. Pie chart areas are proportional to the average mass concentration.

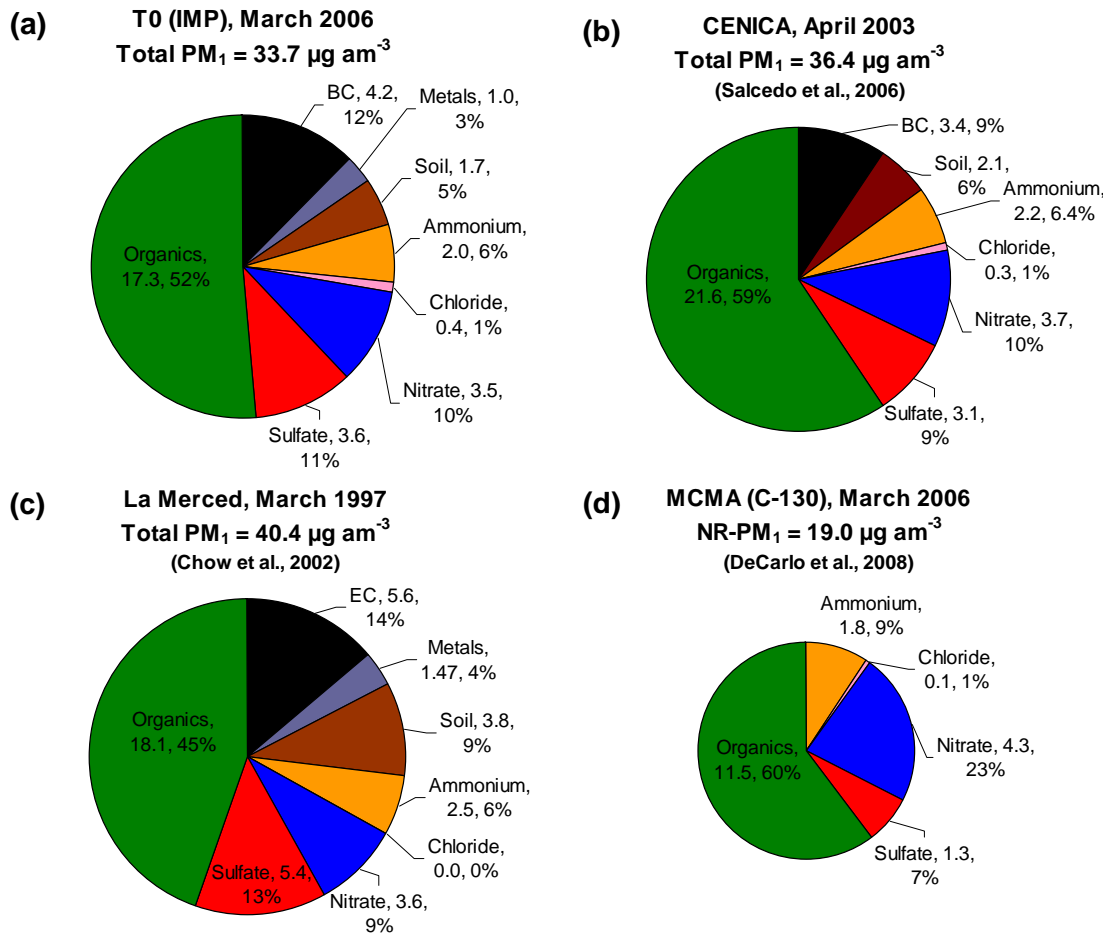


Figure S-9. Average diurnal profiles for (a-e) AMS species and (f-h) refractory species at T0, with a comparison to MCMA-2003 data (Salcedo et al. 2006) in the dashed lines.

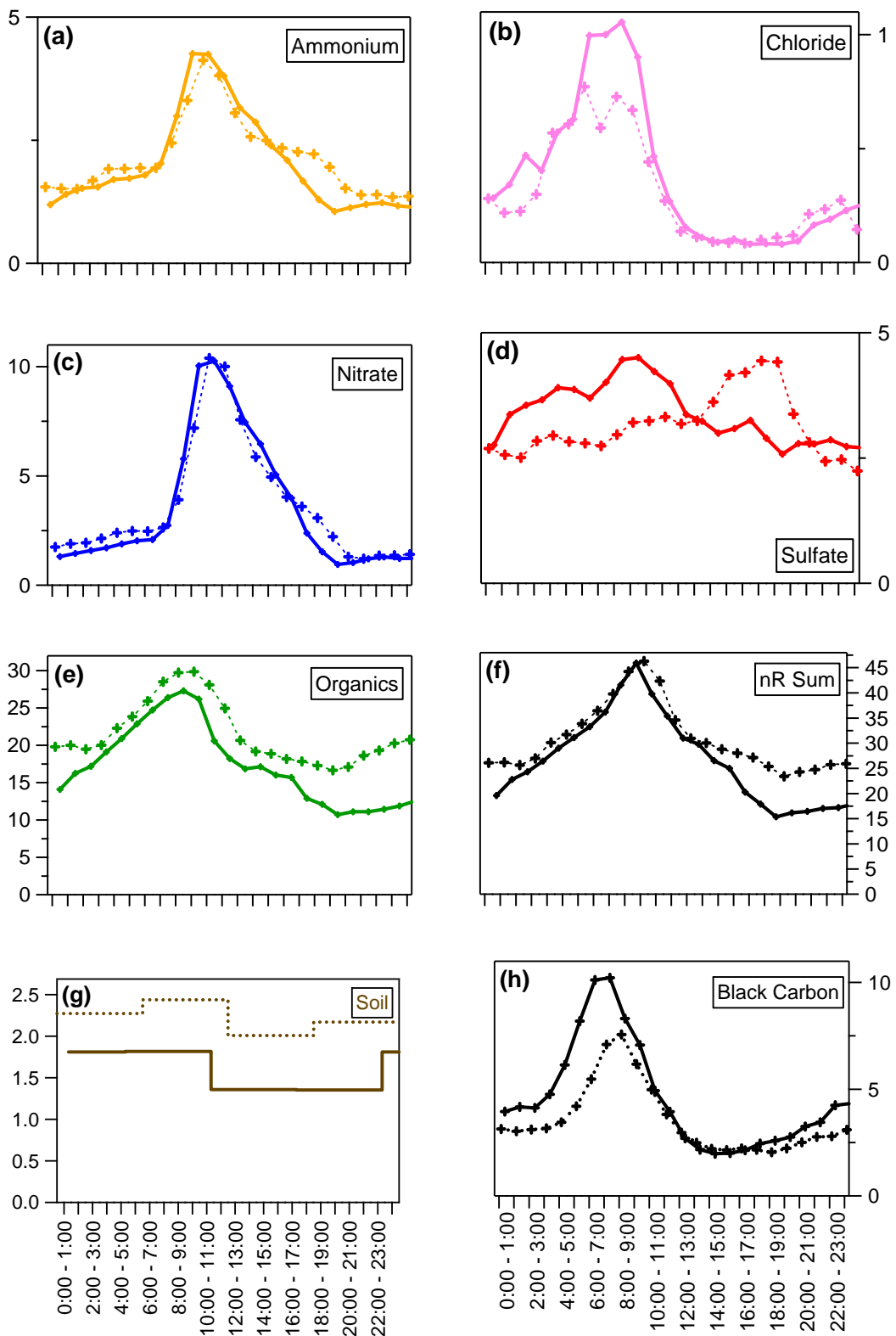


Figure S-10. Average mass spectra with species in standard colors from (a) MILAGRO, T0/IMP and (b) MCMA-2003, CENICA (Salcedo et al. 2006).

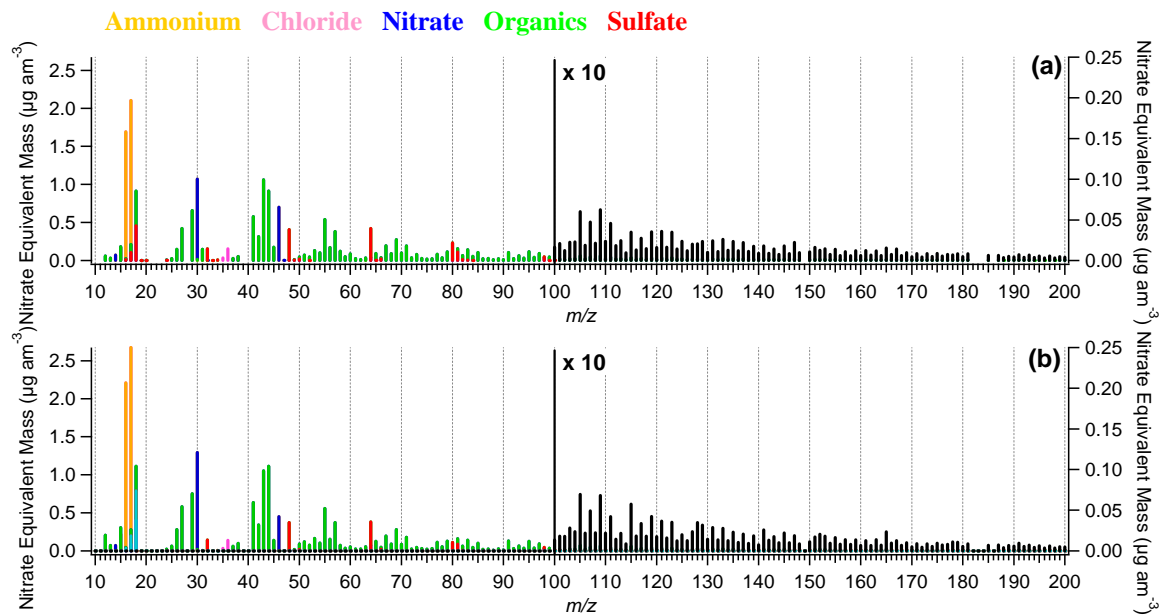


Figure S-11. Size distributions for the AMS chemical species by mass and percent mass from (a,b) T0/IMP (MILAGRO 2006) and (c,d) CENICA (MCMA-2003) by Salcedo et al. (2006).

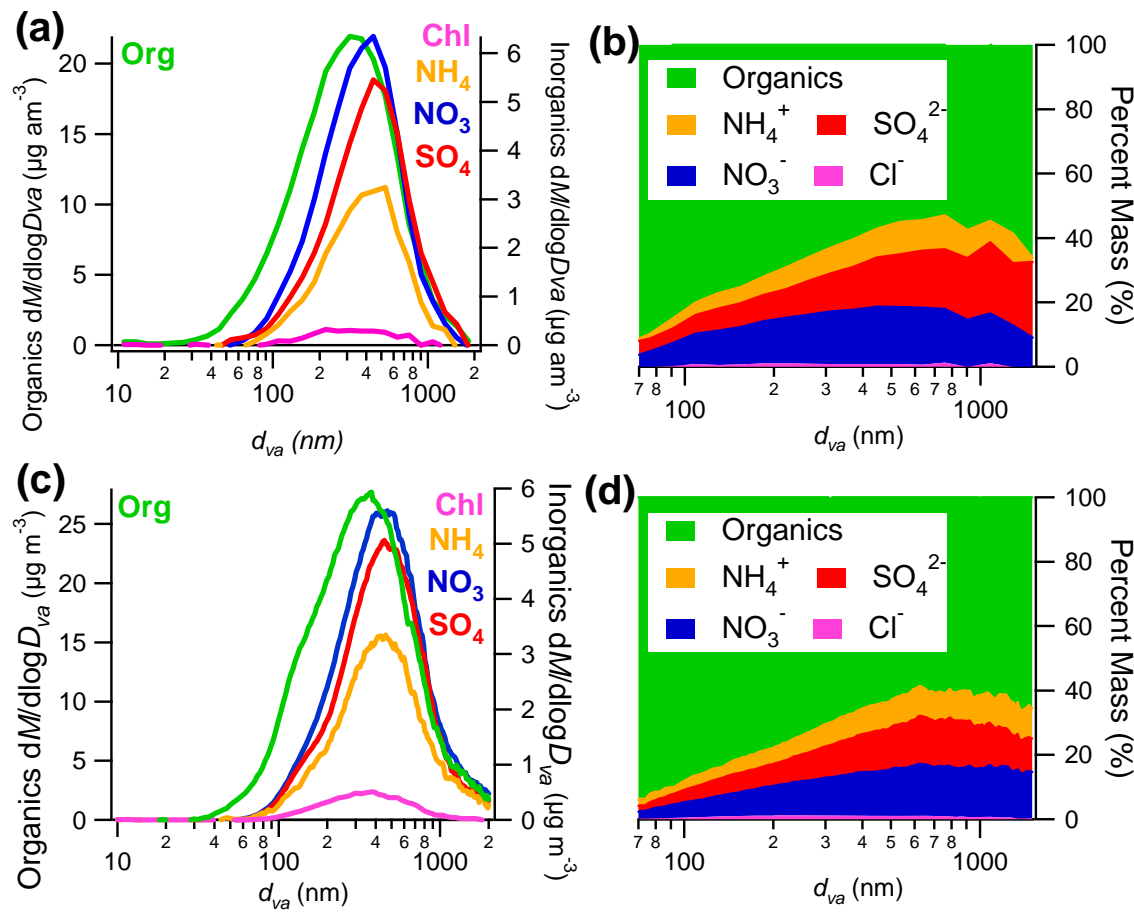
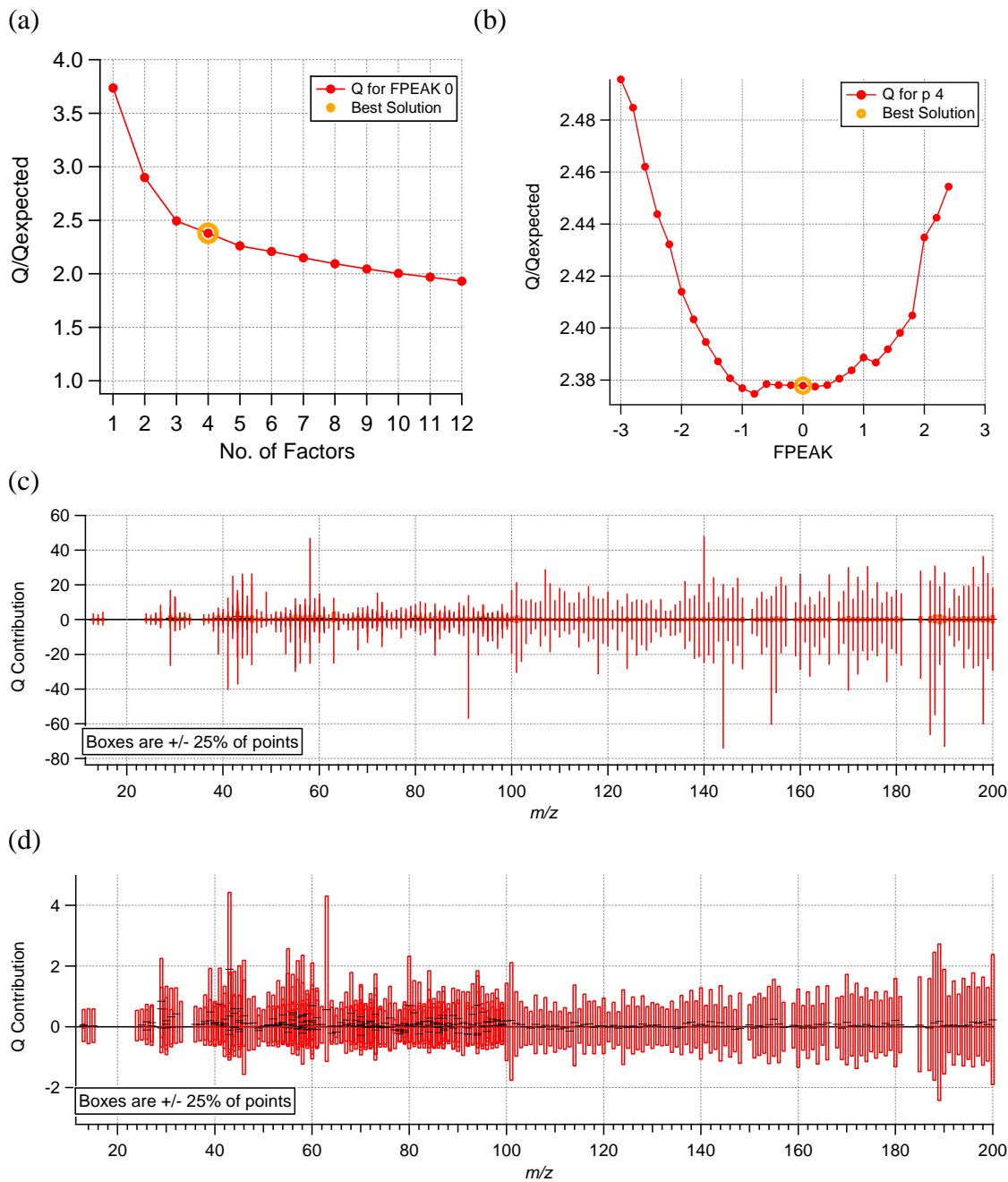
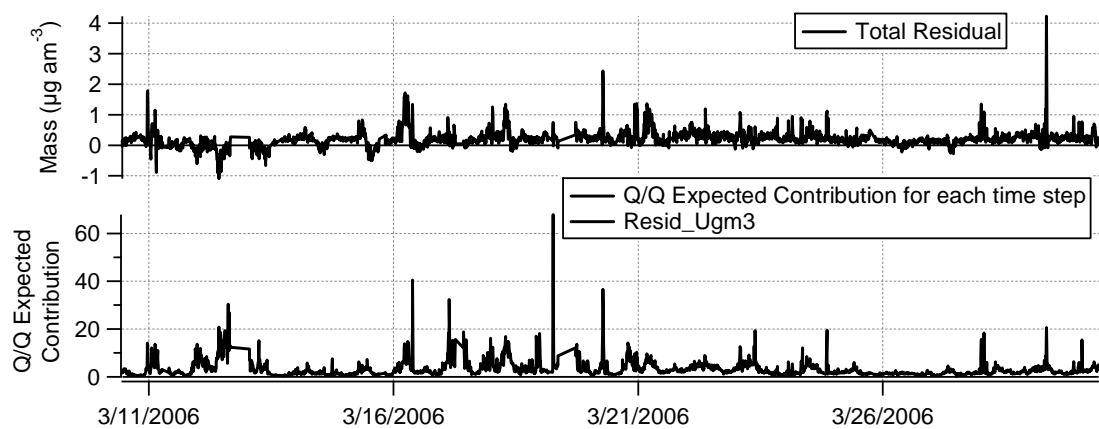


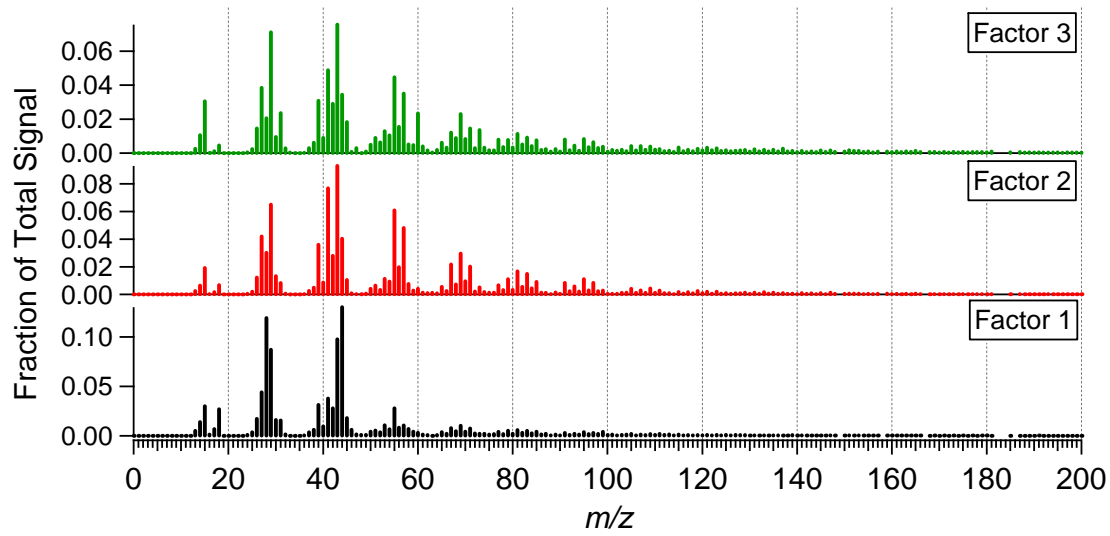
Figure S-12. PMF diagnostic plots: (a) Q/Q expected ($Q =$ the sum of squared scaled residuals over the whole dataset) plotted versus the number of factors used in the PMF solution; (b) Q/Q expected plotted versus the rotational forcing parameter (FPEAK) for solutions with 4 factors; (c,d) box-and-whiskers plots of the scaled residuals; (e,f) time series of the total residual and Q/Q expected contribution for every point in time during the study; (g) factor profiles (mass spectra); and (h) time series the 3-factor solution (with FPEAK = 0); (i) factor profiles and (j) time series for the 5-factor solution (with FPEAK = 0). For more details on PMF and the interpretation of these plots see Ulbrich et al. (2008).



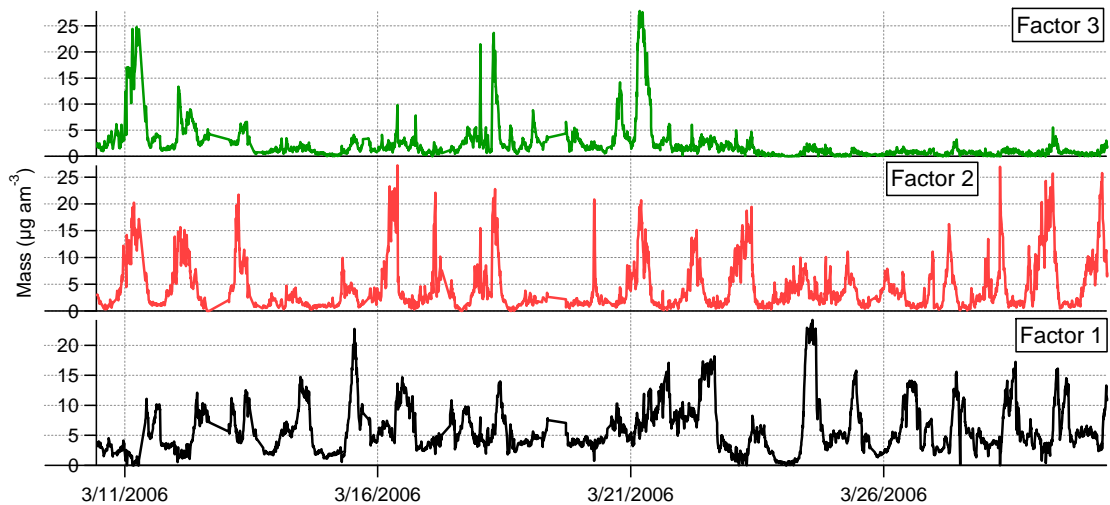
(e,f)



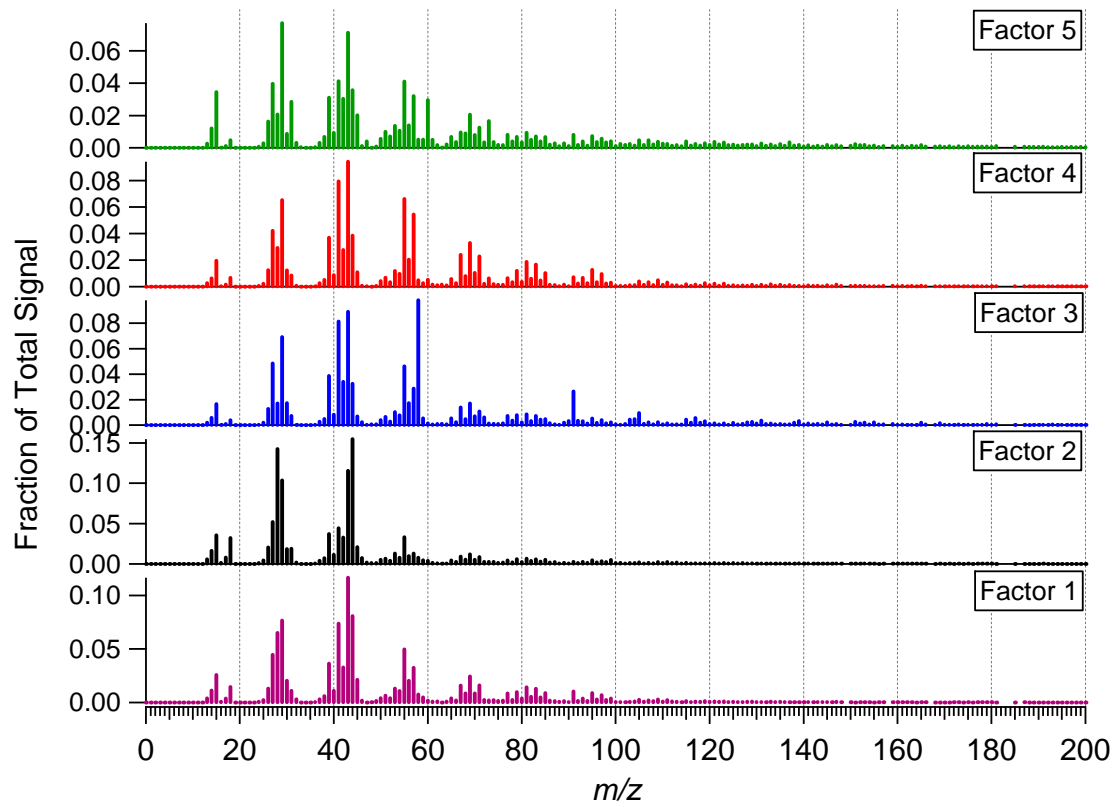
(g)



(h)



(i)



(j)

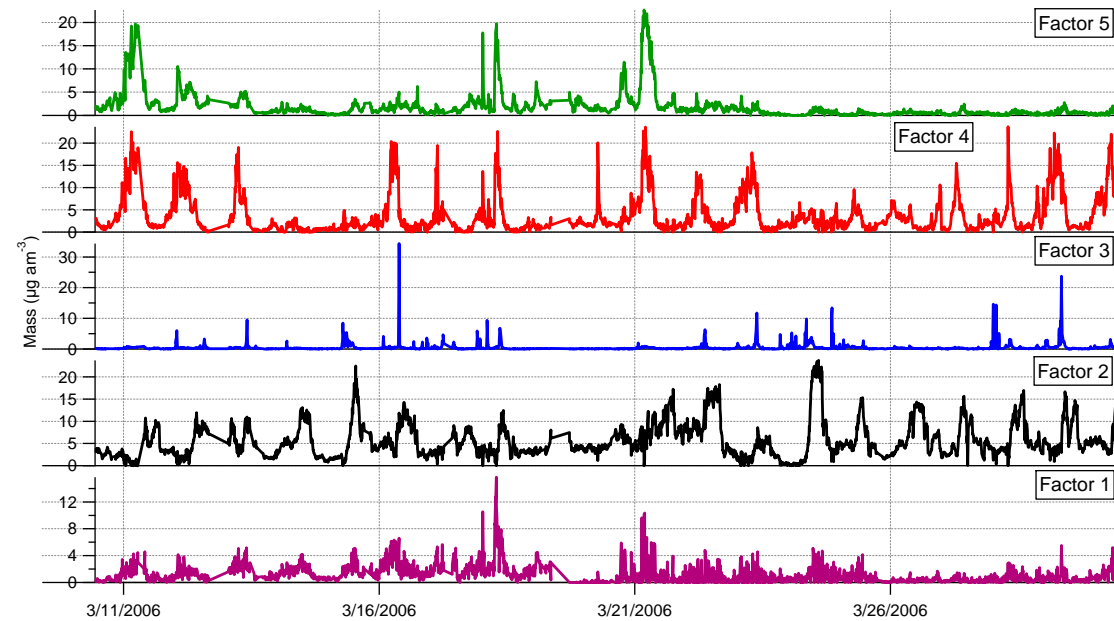


Figure S-13. Time series of (a-d) OA PMF-AMS source mass concentrations and (e) as a percent of total OA. LOA was smoothed by one point from 3/21-25 to remove high-frequency noise.

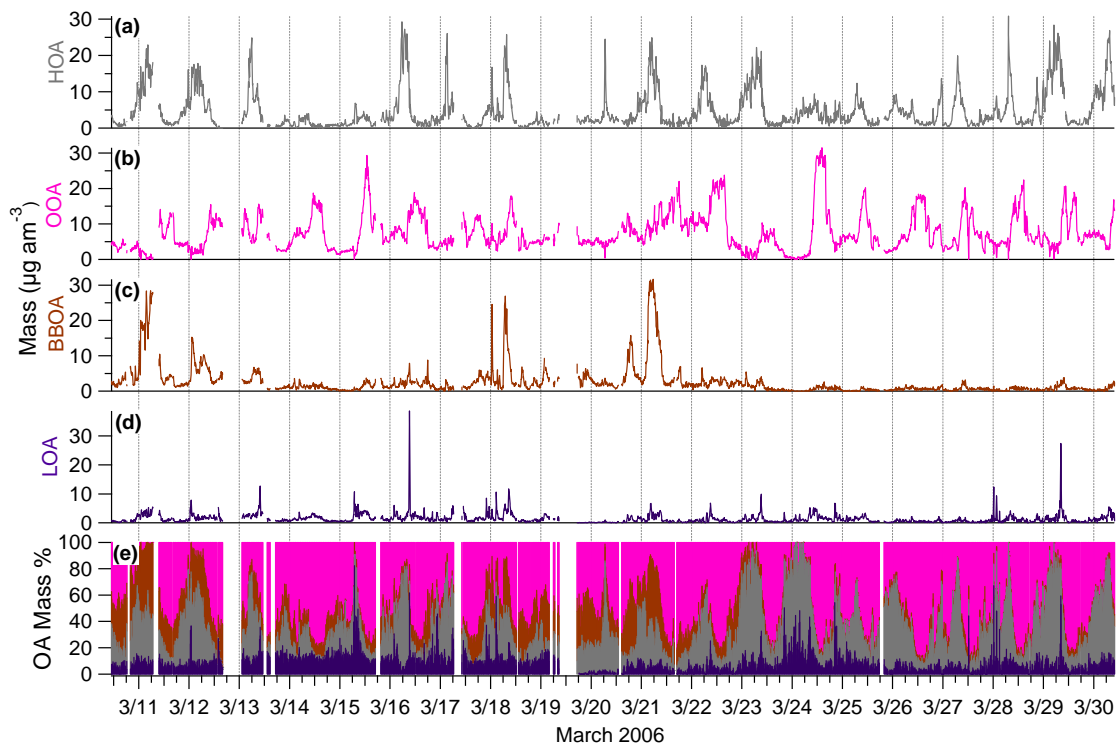
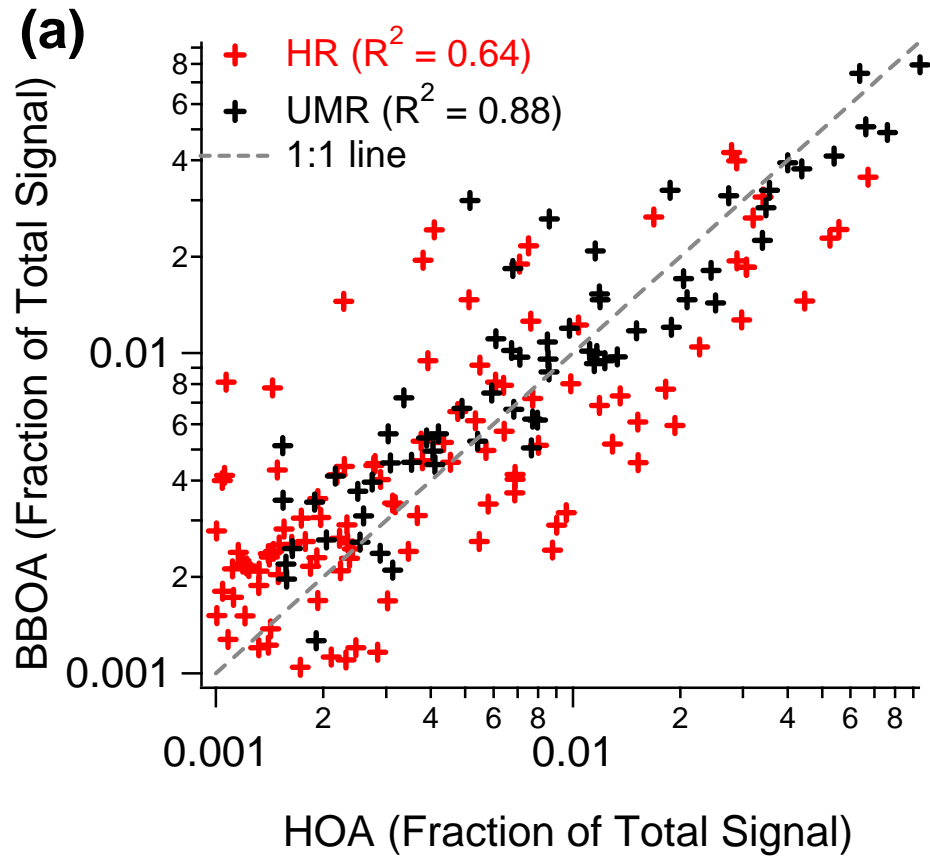


Figure S-14. Scatter plot of MS profiles of BBOA and HOA components for high resolution (HR) and unit mass resolution (UMR) ion signals, scaled as a fraction of the total component MS signal.



Figures S-15. Comparison of HOA mass spectra from (a) Pittsburgh (Zhang et al. 2005) with the fragmentation table of Aiken et al. (2008) applied and (b) MILAGRO, including (c) a scatter plot of the UMR mass spectra with a dashed 1:1 line. High resolution mass spectral signals are colored by ion type.

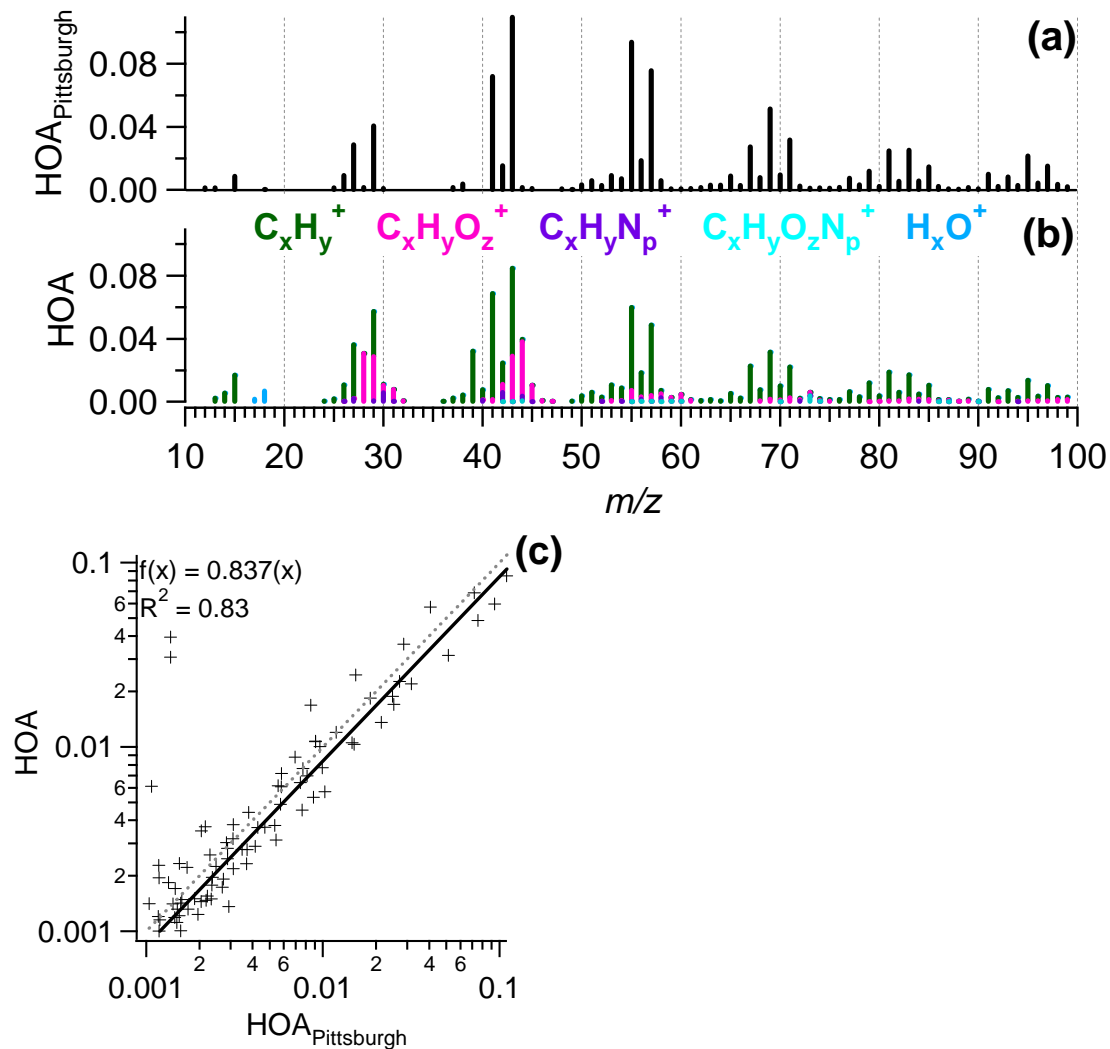


Figure S-16. Comparison of OOA mass spectra from (a) Pittsburgh (Zhang et al. 2005) with the fragmentation table of Aiken et al. (2008) applied and (b) MILAGRO, including (c) a scatter plot of the UMR mass spectra with a dashed 1:1 line. High resolution mass spectral signals are colored by ion type.

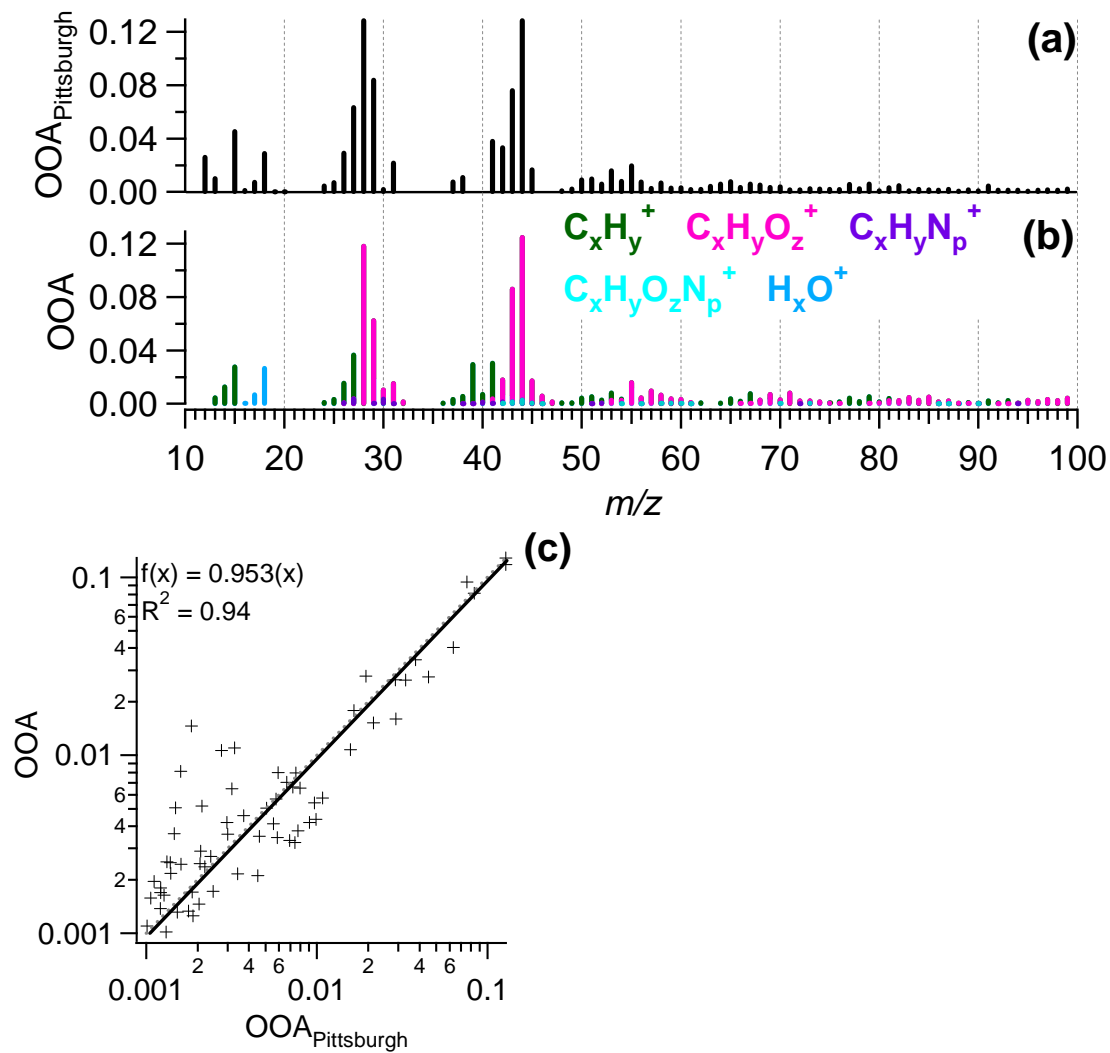


Figure S-17. Autocorrelation plots of the (a-d) four PMF-AMS factors, (e) AMS inorganics, and (f) gas-phase tracers CO, O_x, NO₂.

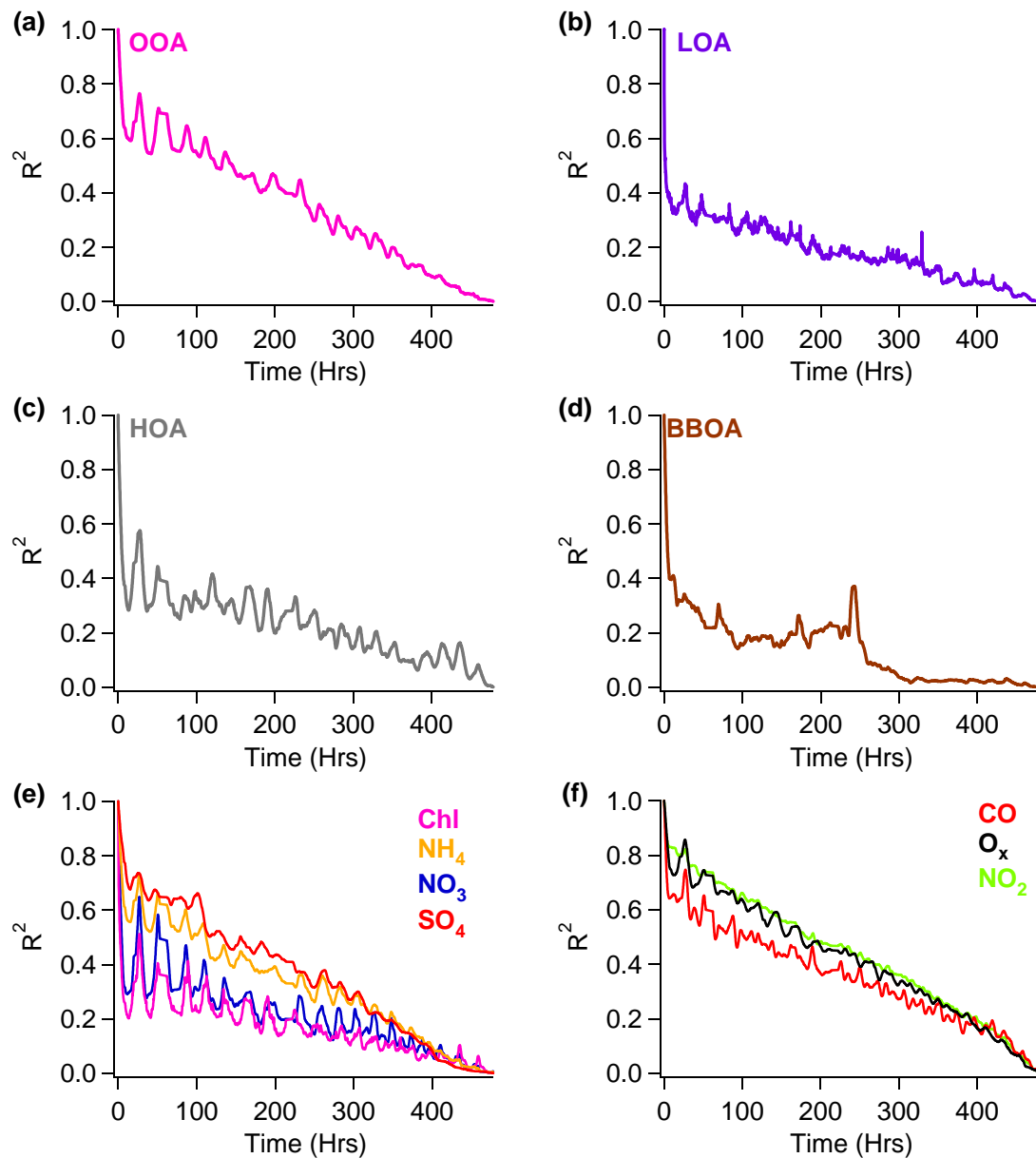
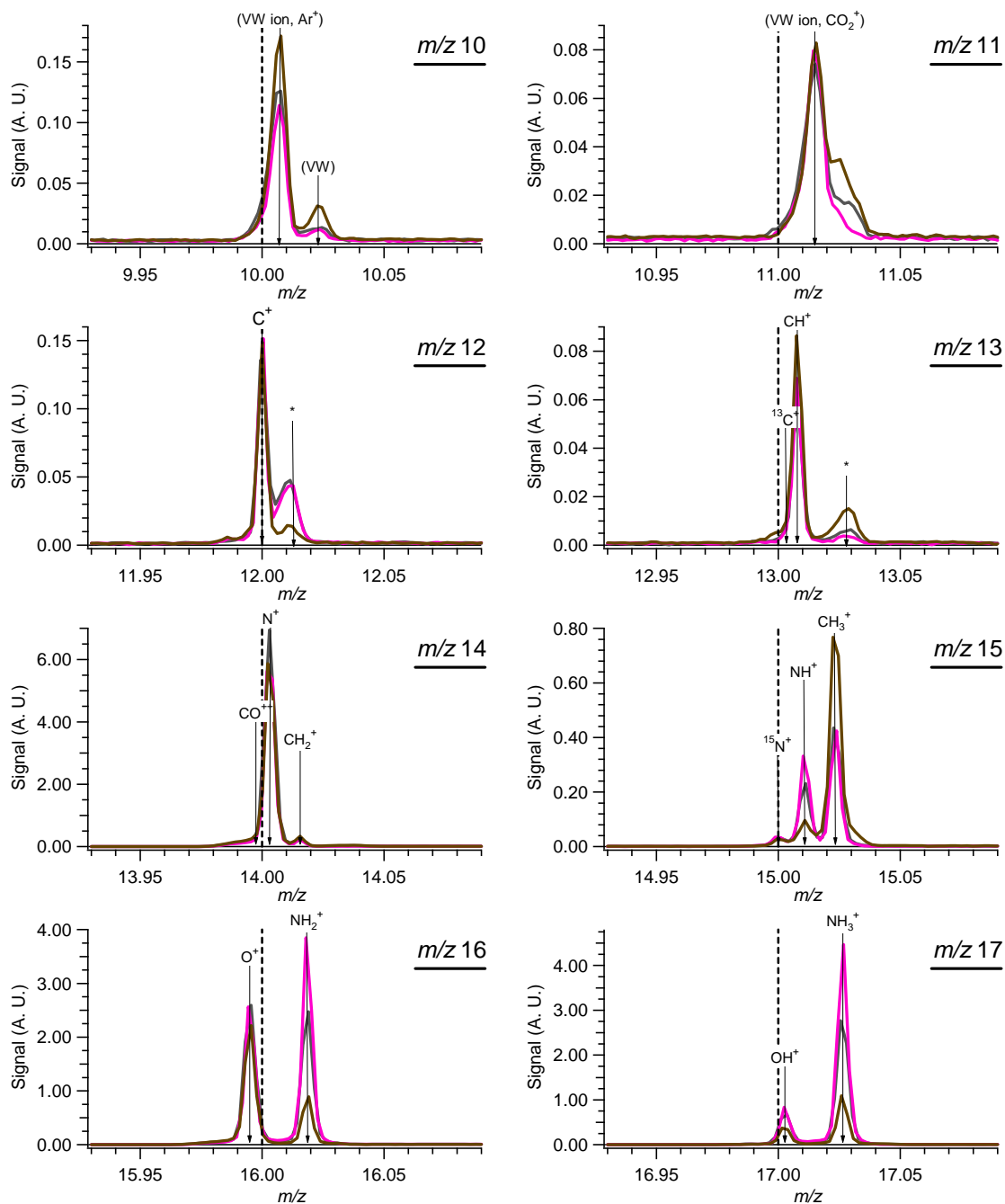
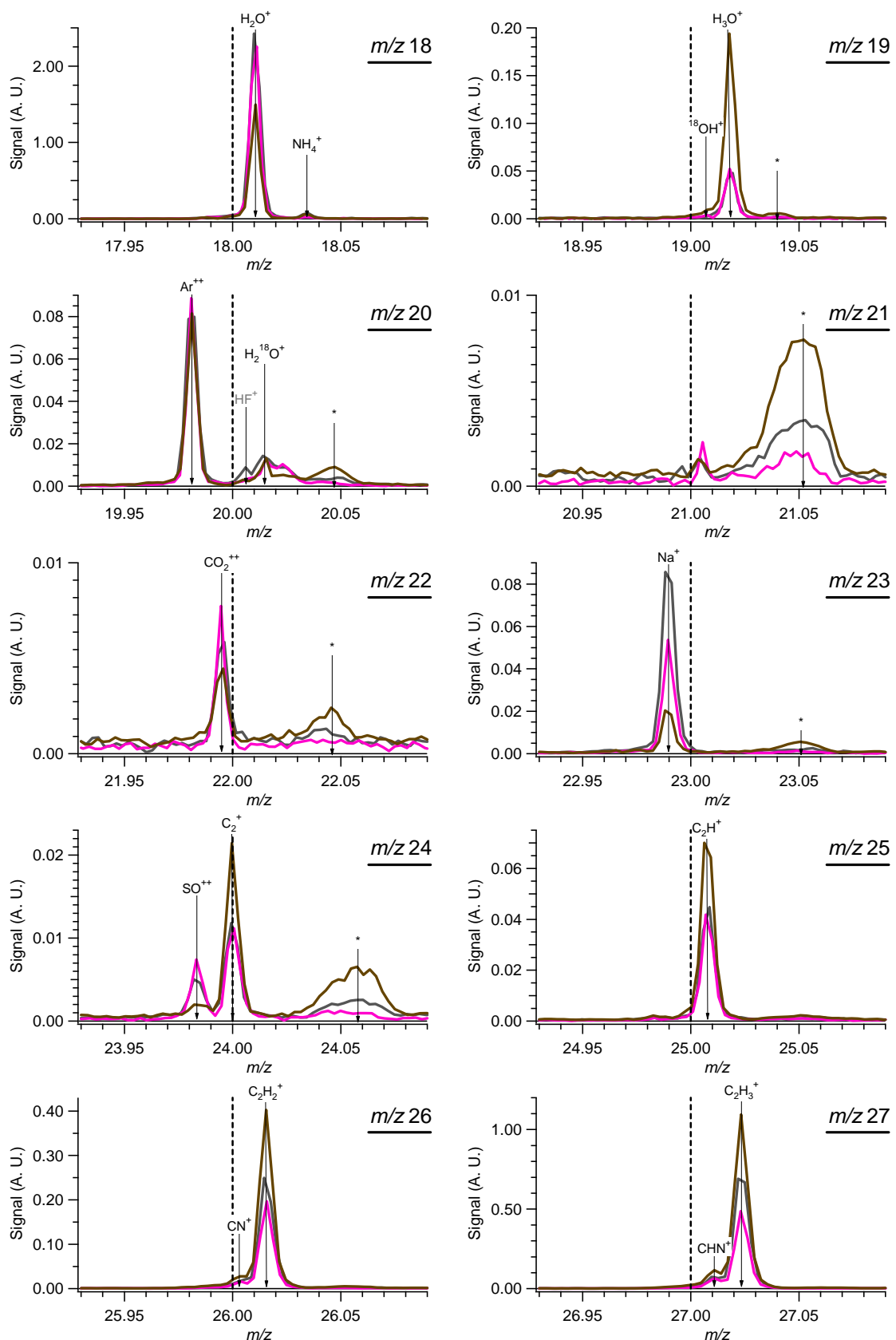
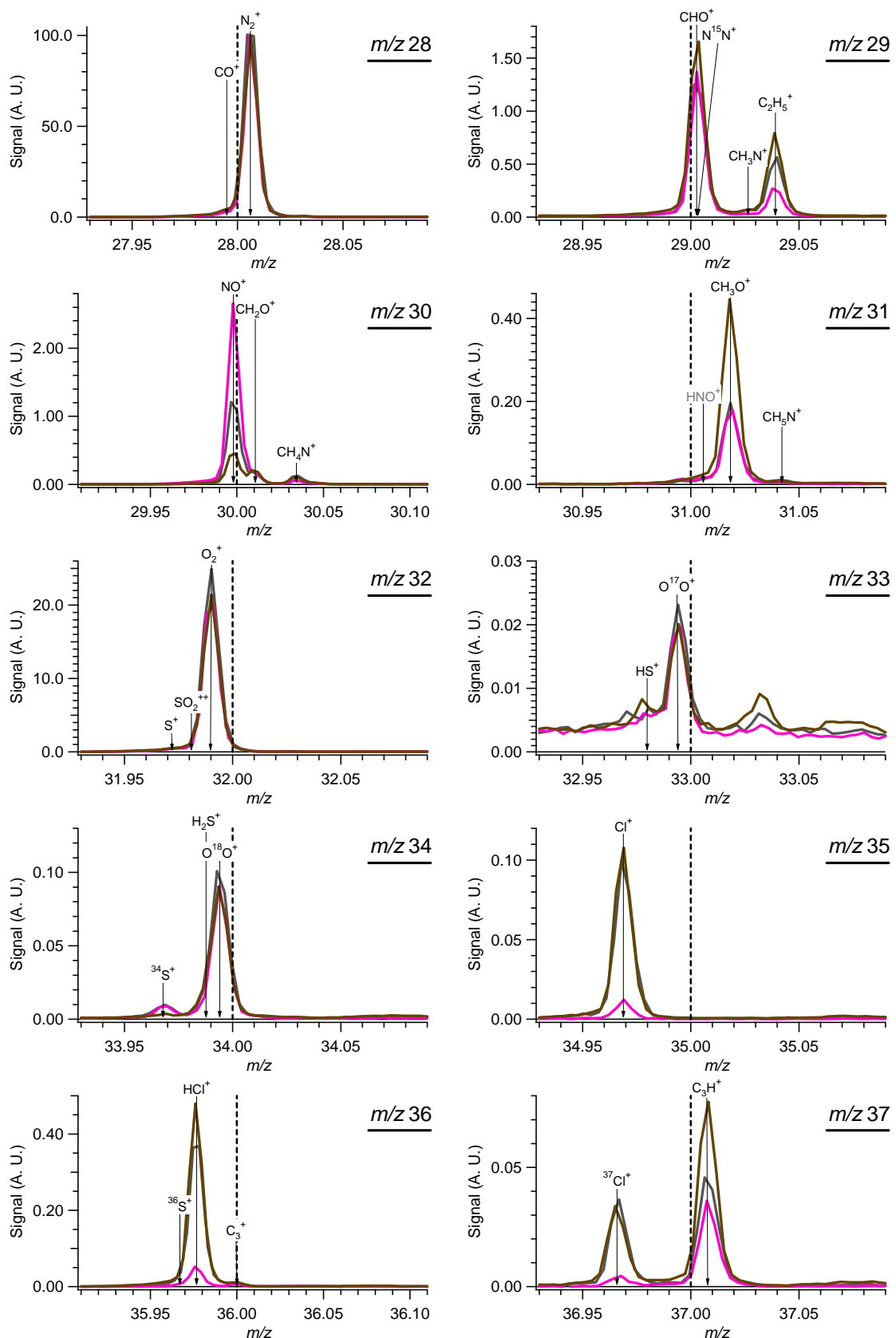
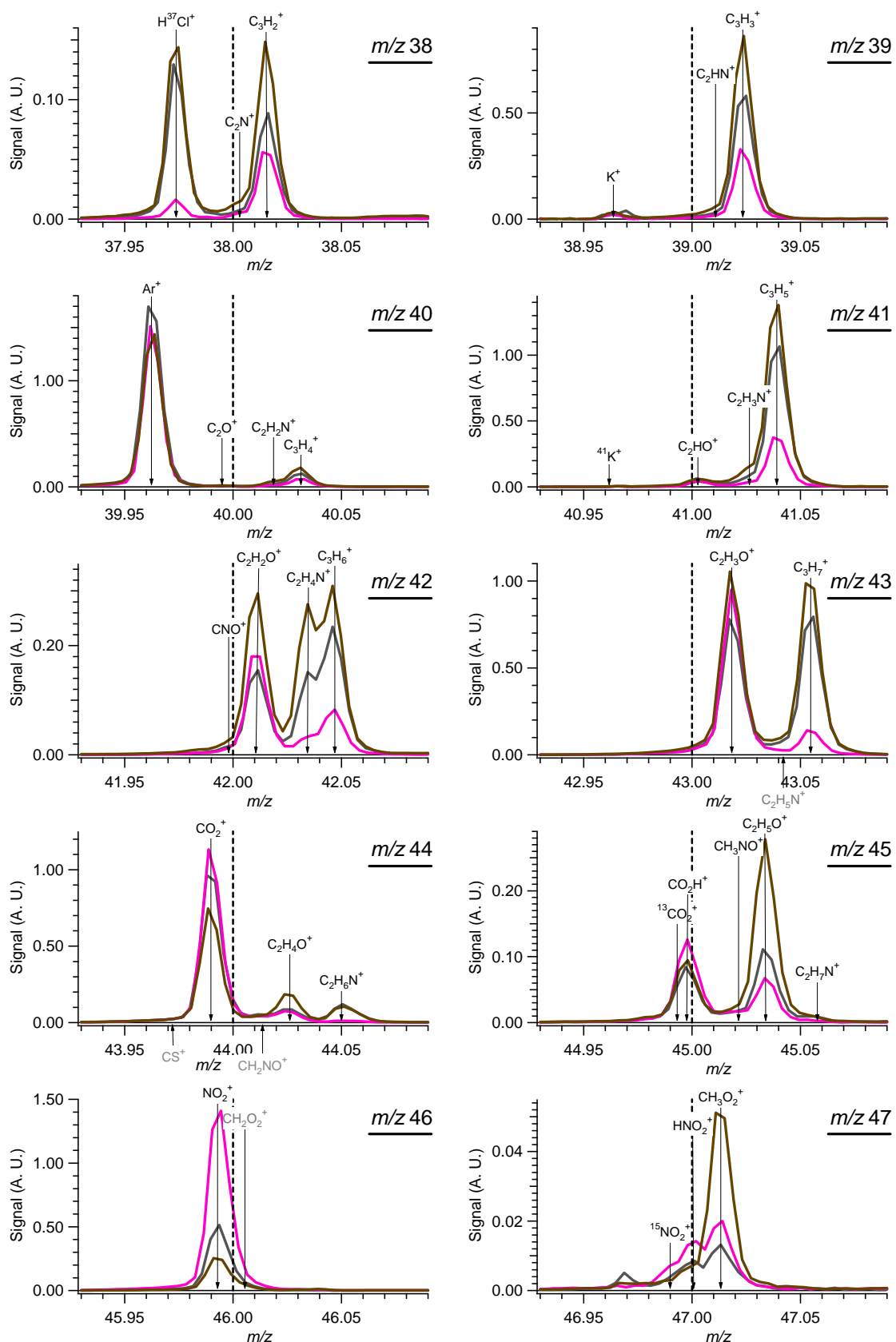


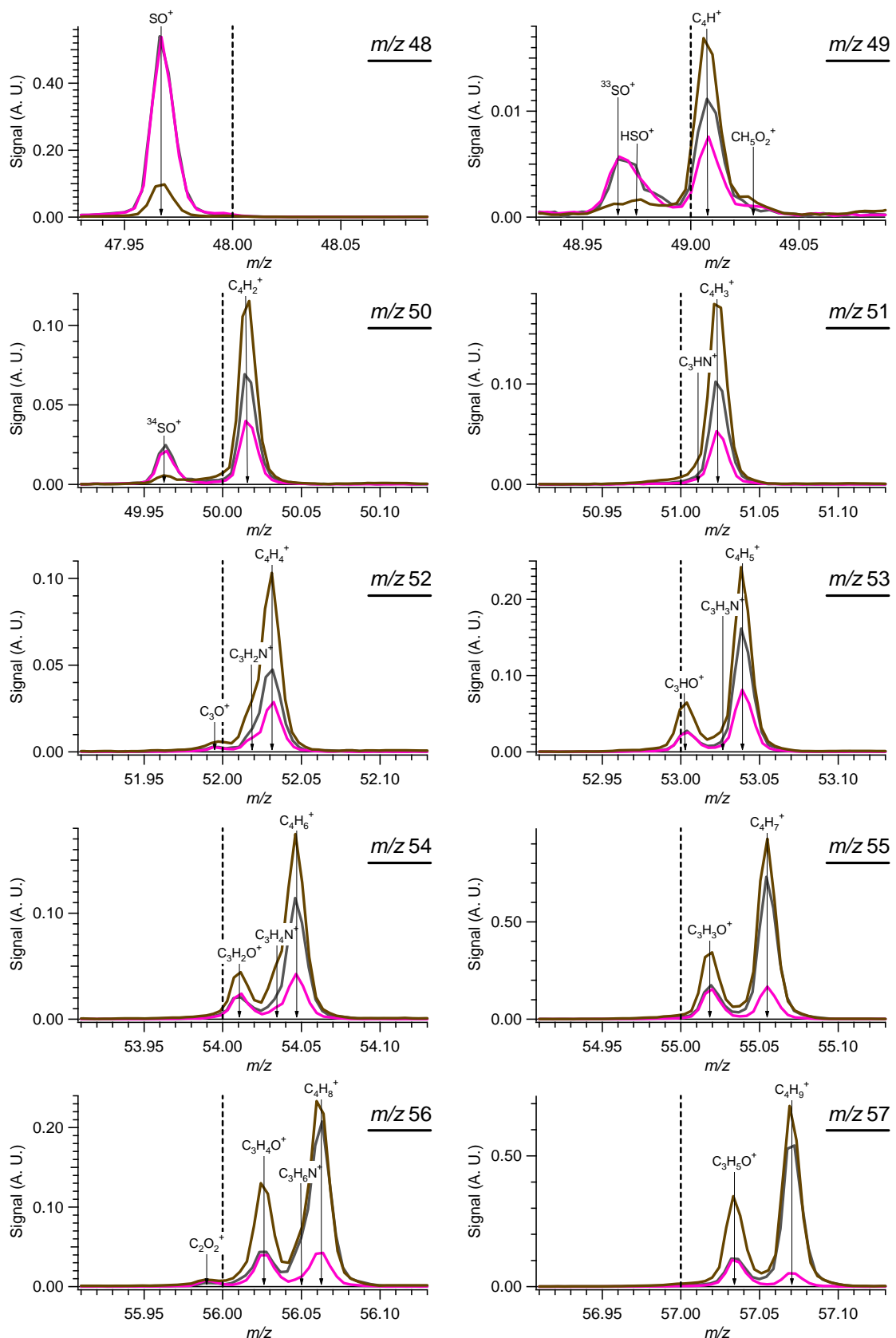
Figure S-18. High resolution ion signals for m/z 's 10 – 100. Signals are averaged over ~5 hours periods when one PMF factor (HOA, BBOA, OOA) dominates the total OA (same periods used in Figure 7) and are scaled to the air signal (N_2^+). (Grey ions are included for reference, but not likely large contributions to the signals. Ions marked with an asterisks are not identified, and at least some of them arise from small artifacts of the mass spectrometer, such as ions that follow a V-mode path while sampling in W-mode.

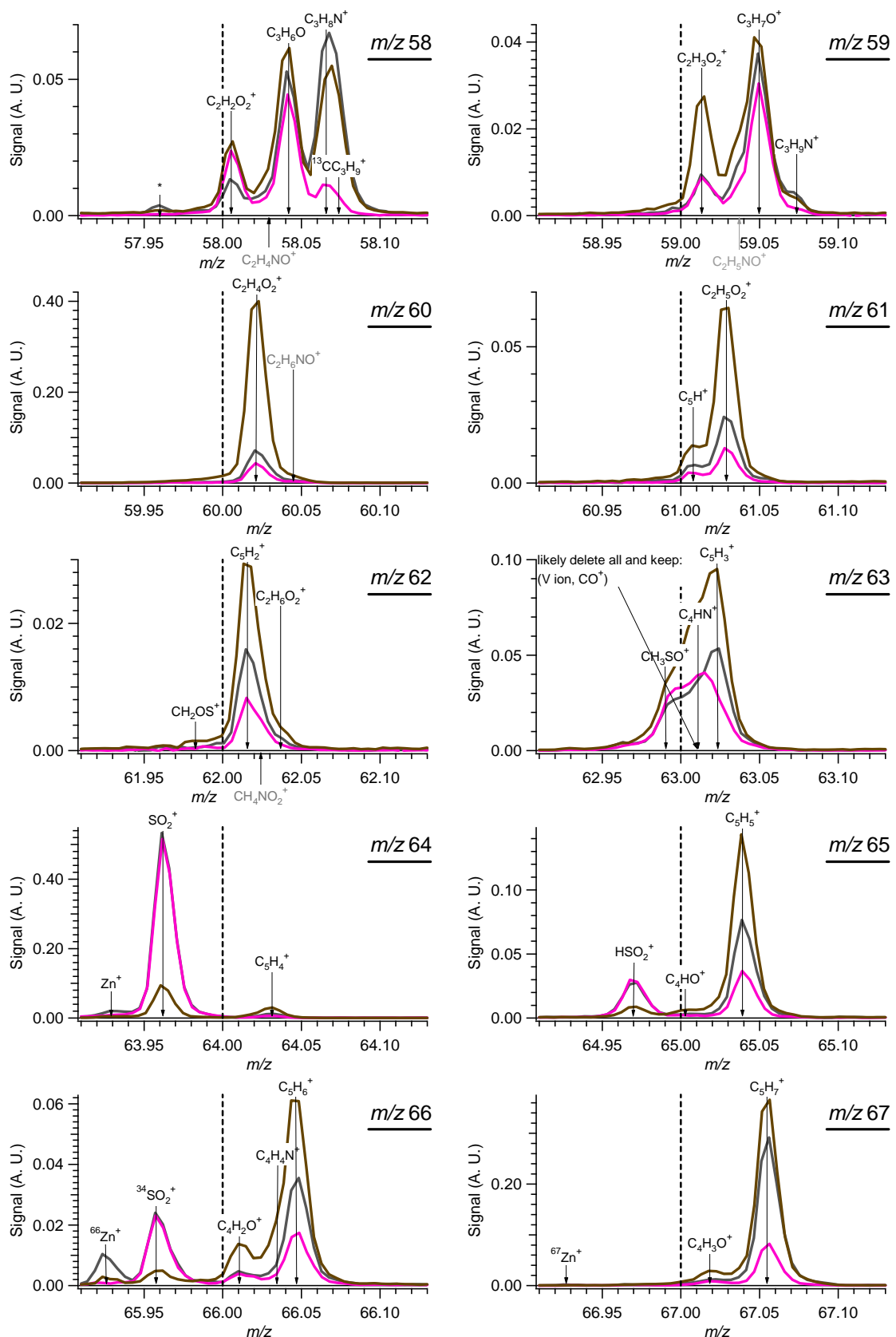


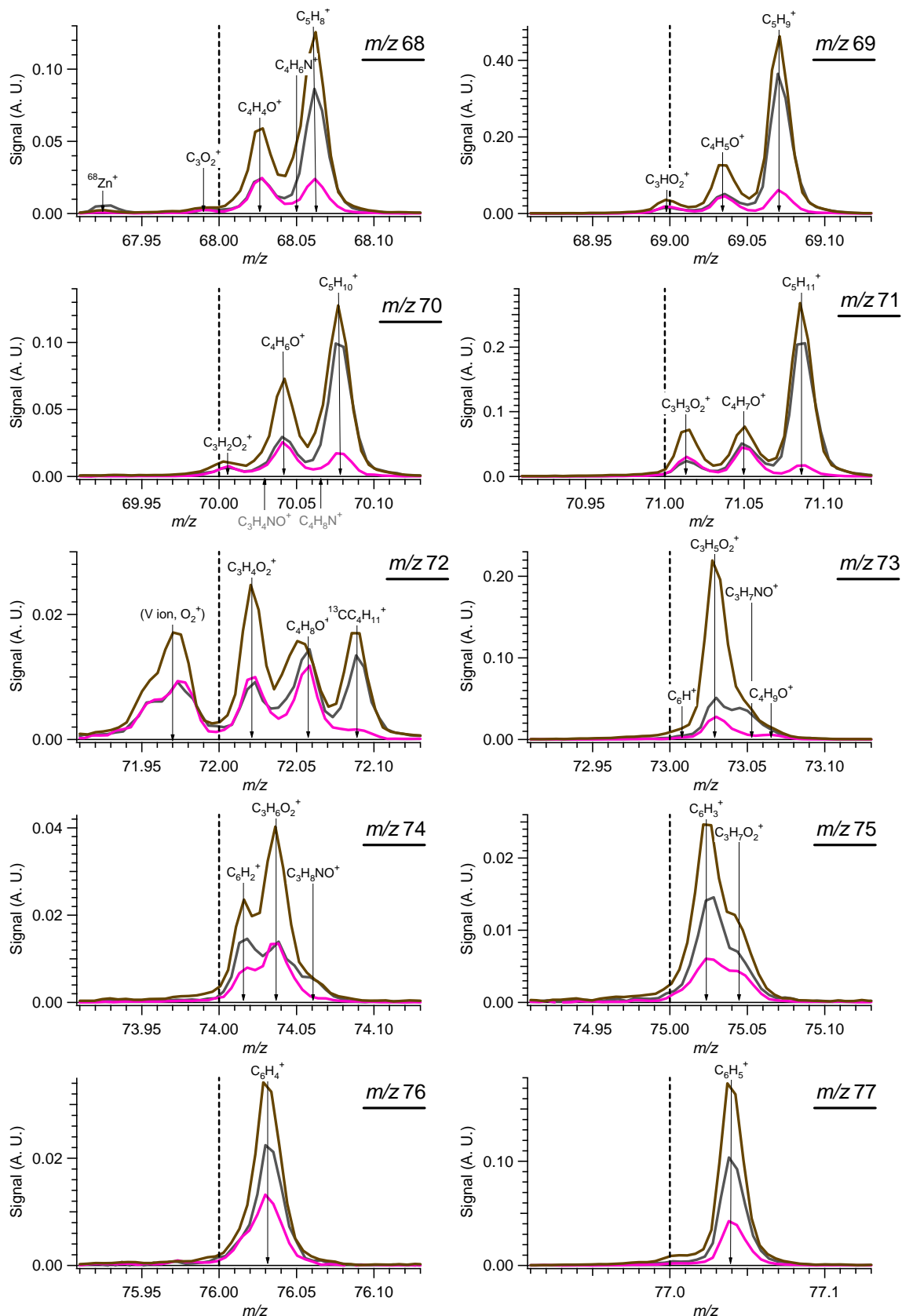


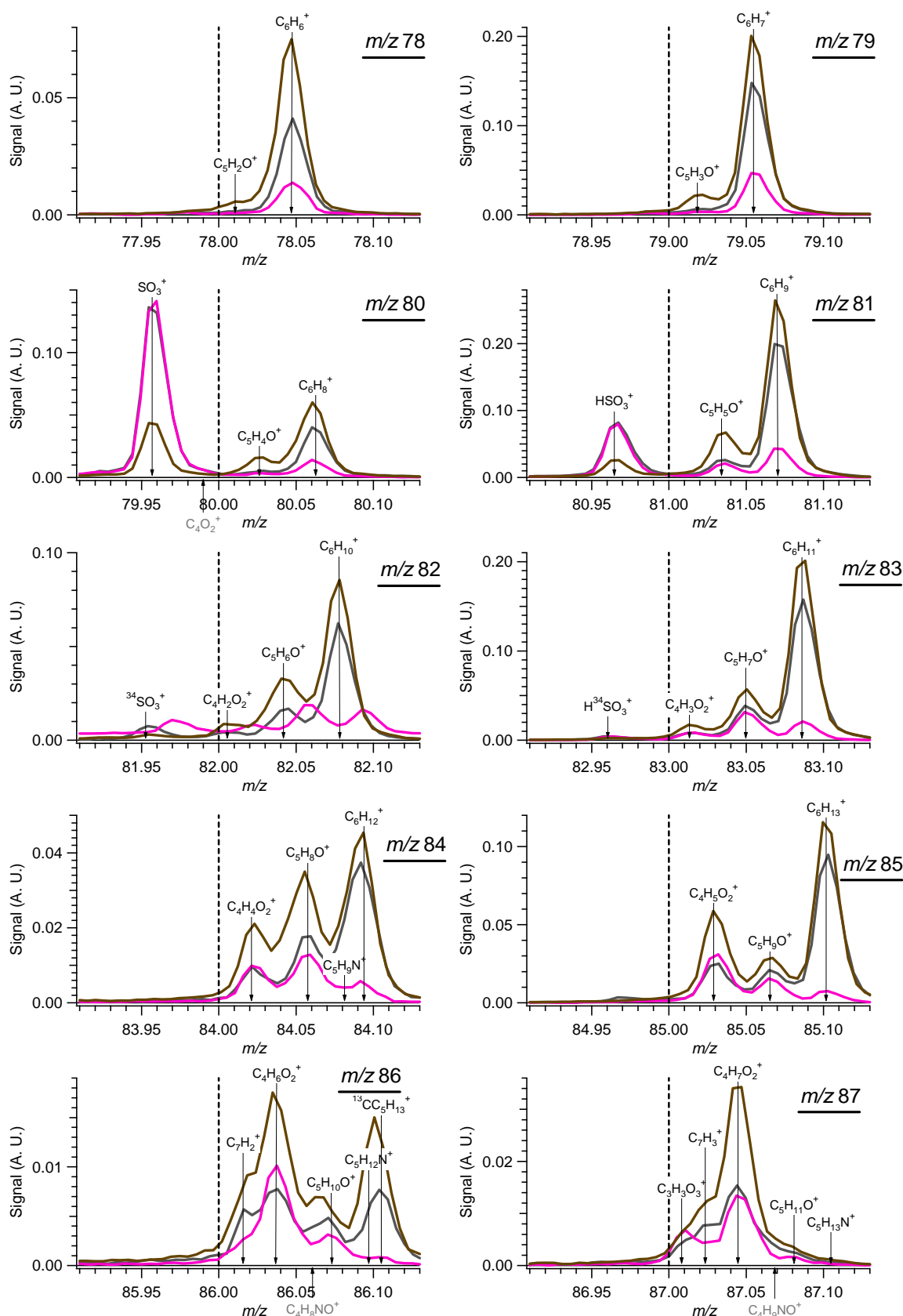


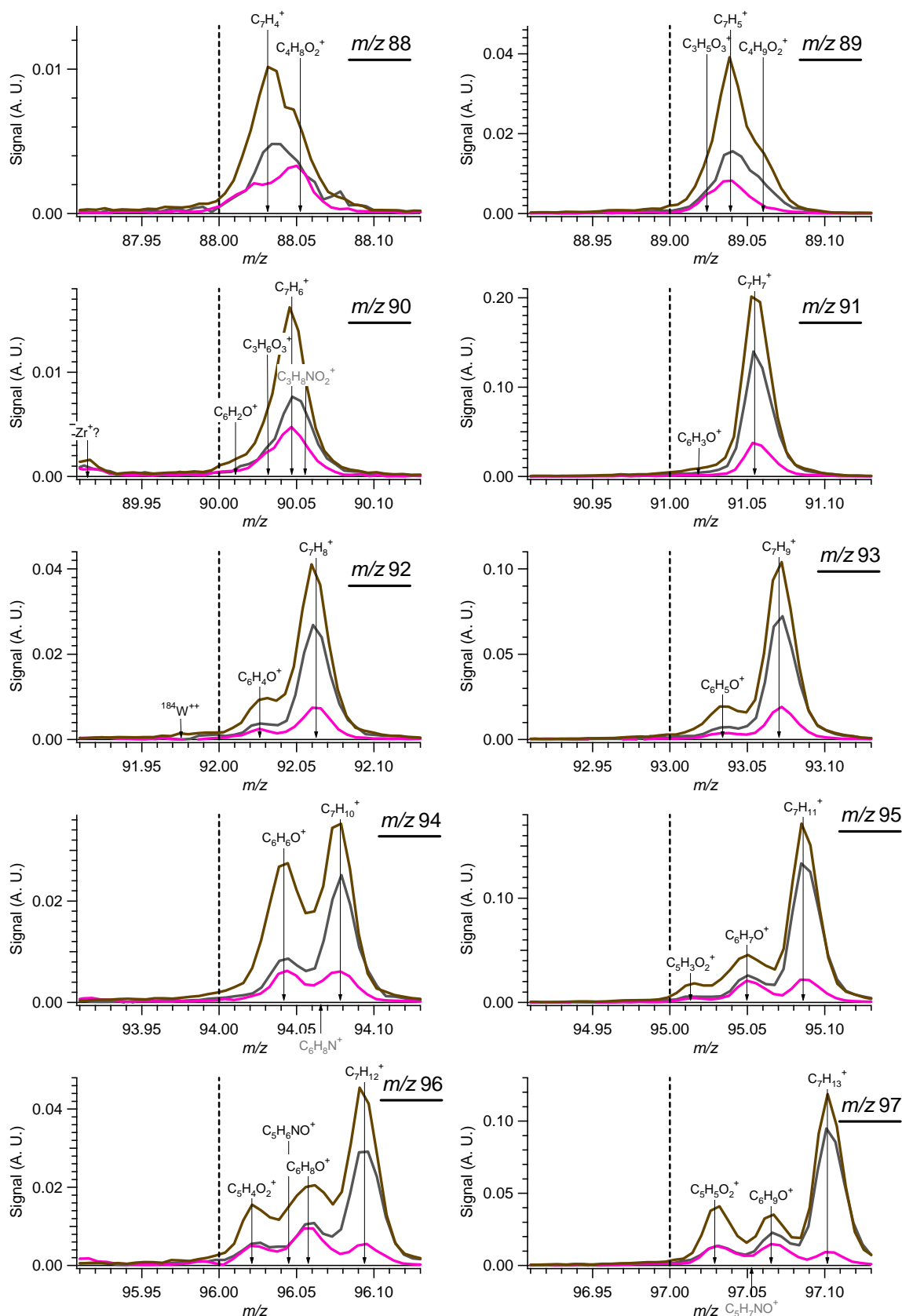


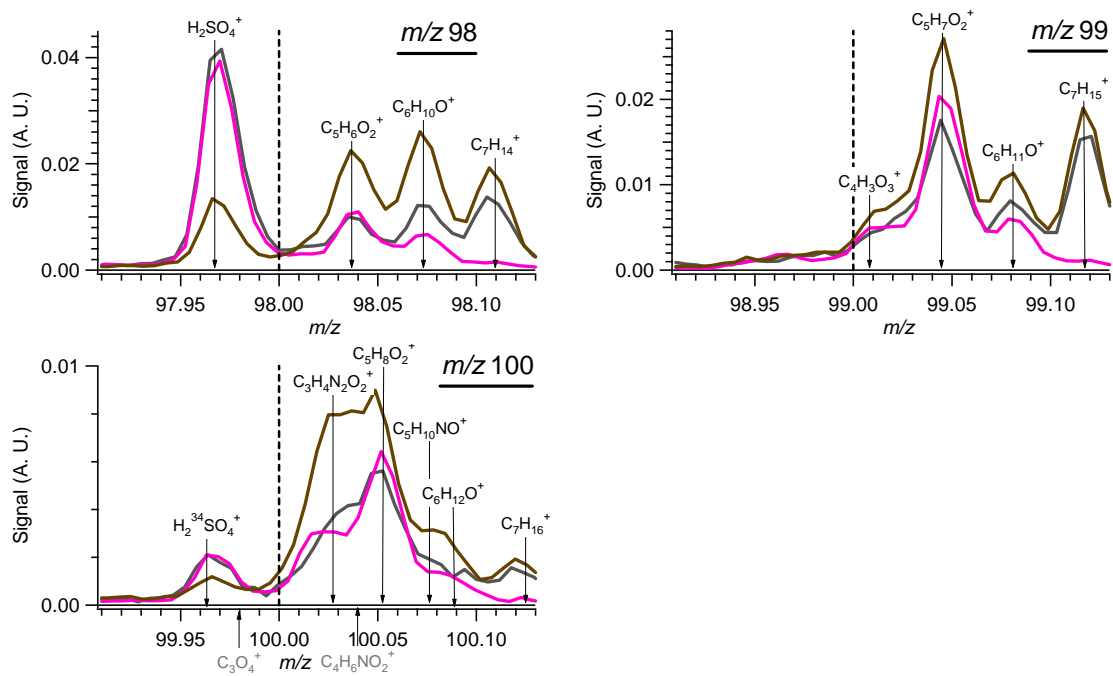












References for Supplementary Information Section:

- Aiken, A.C., P.F. DeCarlo, J.H. Kroll, et al. O/C and OM/OC Ratios of Primary, Secondary, and Ambient Organic Aerosols with High-Resolution Time-of-Flight Aerosol Mass Spectrometry. *Environ. Sci. Technol.* 42, 12: 4478-4485; 10.1021/es703009q, 2008.
- Chow, J.C., J.G. Watson, S.A. Edgerton and E. Vega. Chemical composition of PM_{2.5} and PM₁₀ in Mexico City during winter 1997. *Sci. Total Environ.* 287, 3: 177-201, 2002.
- Moffet, R.C., B. de Foy, L.T. Molina, M.J. Molina and K.A. Prather. Measurement of ambient aerosols in northern Mexico City by single particle mass spectrometry. *Atmos. Chem. Phys.* 8: 4499-4516, 2008.
- Salcedo, D., T.B. Onasch, K. Dzepina, et al. Characterization of ambient aerosols in Mexico City during the MCMA-2003 campaign with Aerosol Mass Spectrometry: results from the CENICA Supersite. *Atmos. Chem. Phys.* 6: 925-946, 2006.
- Ulbrich, I.M., M. Canagaratna, Q. Zhang, D.R. Worsnop and J.L. Jimenez. Interpretation of organic components from positive matrix factorization of aerosol mass spectrometric data. *Atmos. Chem. Phys. Discuss.* 8, 2: 6729-6791, 2008.
- Zhang, Q., M.R. Alfarra, D.R. Worsnop, J.D. Allan, H. Coe, M.R. Canagaratna and J.L. Jimenez. Deconvolution and quantification of hydrocarbon-like and oxygenated organic aerosols based on aerosol mass spectrometry. *Environ. Sci. Technol.* 39, 13: 4938-4952, 2005.